Biomedicine & Pharmacotherapy 167 (2023) 115537

Contents lists available at ScienceDirect

Biomedicine & Pharmacotherapy

journal homepage: www.elsevier.com/locate/biopha

Anti-inflammatory and immunomodulating effects of rilpivirine: Relevance for the therapeutics of chronic liver disease

Angela B. Moragrega [a,b,1], Aleksandra Gruevska [a,b,1], Isabel Fuster-Martínez [a,b], Ana M. Benedicto [a,b], Joan Tosca [c], Cristina Montón [c], Victor M. Victor [b,d,e,f], Juan V. Esplugues [a,b,d], Ana Blas-García [b,d,f,*,2], Nadezda Apostolova [a,b,d,*,2]

[a] Departamento de Farmacología, Facultad de Medicina, Universidad de Valencia, Valencia, Spain
[b] FISABIO–Hospital Universitario Dr. Peset, Valencia, Spain
[c] Departmento de Medicina Digestiva, Hospital Clínico Universitario de Valencia, Valencia, Spain
[d] Centro de Investigación Biomédica en Red de Enfermedades Hepáticas y Digestivas (CIBERehd), Spain
[e] Fundación para la Investigación del Hospital Clínico de la Comunidad Valenciana (INCLIVA), Valencia, Spain
[f] Departamento de Fisiología, Facultad de Medicina, Universidad de Valencia, Valencia, Spain

ARTICLE INFO

Keywords:
Liver disease
Inflammation
Rilpivirine
Leukocytes
Macrophages

ABSTRACT

Non-alcoholic fatty liver disease (NAFLD) is the most common cause of chronic liver disease (CLD) worldwide and inflammation is key to its progression/resolution. As we have previously described that rilpivirine (RPV) is hepatoprotective in murine models of CLD, here we determine the molecular mechanisms involved, focusing on its anti-inflammatory and immunomodulating properties. They were evaluated *in vitro* (human hepatic cell lines of the major hepatic cell types), *in vivo* (liver samples from a murine nutritional model of NAFLD) and *ex vivo* (peripheral blood mononuclear cells -PBMC- from patients with CLD). Transcriptomic analysis of liver samples from NAFLD mice showed RPV down-regulated biological processes associated with the inflammatory response (NF-κB/IκB signaling and mitogen-activated protein kinase -MAPK- activity) and leukocyte chemotaxis and migration. We observed a decrease in *Adgre1* and *Ccr2* expression and in the number of CCR2 + cells in the periportal areas of RPV-treated NAFLD mice. This RPV-induced effect on the CCL2/CCR2 axis was confirmed *in vitro*. A similar result was also obtained with CXCL10/IP10, one of the main chemokines in the liver. RPV also diminished activation of MAP kinases p38 and JNK. In addition, RPV inhibited the NLRP3 inflammasome pathway *in vitro*, decreasing NLRP3 protein expression, caspase-1 activation and *IL-1*β gene expression. RPV was also proven anti-inflammatory in PBMC from patients with CLD treated *ex vivo*. In conclusion, beyond its well-described role in antiretroviral therapy, RPV manifests anti-inflammatory and immunoregulatory effects, a finding that could be of great relevance for the search of novel targets or repositioning strategies for CLD.

1. Introduction

Chronic liver disease (CLD) is a process of continuous and progressive deterioration of the liver function which occurs through inflammation, destruction and compensatory regeneration of liver parenchyma, liver fibrosis (LF), and in a later stage can lead to cirrhosis and hepatocellular carcinoma (HCC). CLD is highly prevalent worldwide [1] and accounts for approximately 2 million deaths per year, half of which are due to complications of cirrhosis [2]. The spectrum of etiologies for CLD is broad and includes prolonged exposure to hepatotoxins,

Abbreviations: CLD, chronic liver diseases; Col1a1, collagen type I alpha I; DAMP, damage associated molecular patterns; HFD, high fat diet; HIV, human immunodeficiency virus; HSC, hepatic stellate cells; IL, interleukin; JAK, Janus kinase; JNK, c-Jun N-terminal kinase; LPS, lipopolysaccharide; LF, liver fibrosis; MAPK, mitogen-activated protein kinases; MMP, matrix metalloproteinase; NAFLD, non-alcoholic fatty liver disease; NASH, non-alcoholic steatohepatitis; ND, normal diet; NF-κB, nuclear factor kappa B; NLRP3, NOD-like receptor family pyrin domain containing 3; RPV, rilpivirine; α-SMA, alpha-smooth muscle actin; STAT, signal transducer and activator of transcription; TGF-β, transforming growth factor β; TNF-α, tumor necrosis factor α.

* Correspondence to: Departamento de Farmacología y Departmento de Fisiología, Universitat de València.
E-mail addresses: ana.blas@uv.es (A. Blas-García), nadezda.apostolova@uv.es (N. Apostolova).

[1] These authors have contributed equally
[2] These authors have contributed equally

https://doi.org/10.1016/j.biopha.2023.115537
Received 18 July 2023; Received in revised form 14 September 2023; Accepted 17 September 2023
Available online 20 September 2023
0753-3322/© 2023 The Authors. Published by Elsevier Masson SAS. This is an open access article under the CC BY-NC-ND license (http://creativecommons.org/licenses/by-nc-nd/4.0/).

alcohol abuse, viral infection (HBV and HCV), autoimmune diseases, and genetic and metabolic disorders. Non-alcoholic fatty liver disease (NAFLD) has become the most common form of CLD, with a worldwide prevalence of 25%, thereby representing a great health burden [3]. Importantly, specific pharmacological therapies for NAFLD are still missing. The more progressive stage of NAFLD is non-alcoholic steatohepatitis (NASH) in which inflammation is a pivotal driver, thus mechanisms underlying inflammation in NAFLD/NASH clearly represent promising therapeutic targets [4]. NASH is also characterized by the progressive development of LF, in which excessive and aberrant extracellular matrix is deposited mainly by activated hepatic stellate cells (aHSC). Various intra- and extrahepatic modulators involved in the metabolic injury and inflammatory processes typically lead to the activation of different immune cells, including Kupffer cells (KC), which can adopt an inflammatory phenotype and activate other immune cells by releasing inflammatory cytokines. As inflammation progresses, KC are increasingly replaced by monocyte-derived macrophages (MDM). Hepatic macrophages engage in close interactions with other non-parenchymal cells of the liver, especially HSC; for instance, transforming growth factor β1 (TGF-β1) and platelet derived growth factor (PDGF) secreted by hepatic macrophages can activate HSC thereby causing LF [5].

The hepatic stress response is sensed by hepatocytes through mitogen-activated protein kinases (MAPK), which transduce extracellular and intracellular signals to regulate cell proliferation, differentiation, apoptosis, and metabolism through terminal kinases such as c-Jun N-terminal kinase (JNK) and p38. JNK activation has been identified as a common pathway in numerous models of liver injury through its relationship with oxidative stress, cell death, inflammation, fibrogenesis and lipotoxic stress [6]. Diets, specifically hypernutrition-type diets, such as high fat and/or high carbohydrate, activate hepatic JNK longer than standard fat and carbohydrate diet.

Recruitment of blood cells to the damaged liver is key in the pathogenesis and resolution of liver injury. CCL2, also known as monocyte chemotactic factor 1 (MCP1), regulates the migration and infiltration of monocytes/macrophages through combination with its specific C-C chemokine receptor type 2 (CCR2). It has been reported that CCL2/CCR2 axis has a vital role during LF [7]. CCL2-dependent infiltrating macrophages promote angiogenesis in progressive LF and CCR2 is mainly responsible for recruiting pro-inflammatory and profibrogenic infiltrating monocytes during LF progression [8].

We have already described that rilpivirine (RPV), an antiretroviral drug widely employed in the treatment of HIV infection, is hepatoprotective, showing antisteatotic and anti-inflammatory effects, and ameliorating LF in different animal models of chronic liver injury [9]. RPV impairs TGF-β-induced activation of cultured HSC, as demonstrated by downregulated expression of general profibrotic markers, and of phosphorylated signal transducer and activator of transcription 3 (pSTAT3), a fibrogenic transcription factor that stimulates HSC survival, proliferation, and activation. In addition, RPV induced apoptosis in aHSC through selective STAT1 activation [9] and this effect involved altered autophagy [10].

Given the implication of the inflammatory and immune response in the development of CLD and the previous findings regarding the mechanisms involved in RPV's action in the liver, the aim of the present study is to investigate the anti-inflammatory and immunomodulating action of this drug both *in vivo* and *in vitro*.

2. Material and methods

2.1. Reagents

Unless stated otherwise, general chemicals were from Sigma-Aldrich. RPV (Sequoia Research Products) was dissolved in DMSO and employed at a final concentration of 1–8 μM. This solvent was used as a control treatment (denoted as "vehicle") and employed for all statistical comparisons.

2.2. Mouse model of fatty liver disease

Animal procedures were performed in accordance with the University of Valencia's guidelines for the care and use of laboratory animals and were approved by the local ethics committee (ref. 2014/VSC/PEA/00188). Female C57BL/6 J mice aged 9 weeks (Janvier Labs) were randomly assigned to different experimentation groups (10 mice per group). Animal dosage was calculated using the normalised interspecies allometric scaling factor established by the Food and Drug Administration (FDA) to achieve the equivalent to the maximum daily therapeutic dose of RPV (25 mg). A nutritional model of NAFLD was employed, for which animals received a normal diet (ND) or a customized high-fat diet (HFD) (Ssniff Labs; EF R/M D12331 mod.*/Surwit; 59% fat and 2% free cholesterol) for 12 weeks, and were administered either RPV (5 mg/kg/day, p.o.) or its vehicle (Veh, DMSO).

2.3. Transcriptomic analysis

The transcriptomic analysis used in the present study was already published [9] and deposited in NCBI Gene Expression Omnibus (accession number GSE120484) [11]. Briefly, RNA expression data came from whole liver samples from a HFD mouse model treated with RPV (comparing hepatic gene expression between HFD mice treated with Veh and HFD mice treated with RPV), and a functional enrichment by gene set analysis (GSA) using Gene Ontology (GO) biological processes [12] was performed. To analyse the mechanisms involved in inflammatory and stress responses processes, the resulted altered GO terms whose adjusted p-value < 0.005 were filtered to those related to the following general GO terms: GO:0006950 (response to stress), GO:0051716 (cellular response to stimulus) and GO:0002376 (immune system process). This analysis was carried out using CateGOrizer web tool, as it classifies the GO terms into groups from a pre-defined list of parent/ancestor GO terms [13].

2.4. Cell culture, treatment and transfections

Human hepatoblastoma Hep3B cells (American Type Culture Collection, ATCC) were cultured in MEM (Gibco, Invitrogen) supplemented with 10% heat-inactivated fetal bovine serum (hi-FBS, Sigma-Aldrich), 1x non-essential amino acid solution, 2 mM L-glutamine and 1 mM sodium pyruvate (all from Gibco, Invitrogen). LX-2, an immortalized cell line of human HSC, (Sigma-Aldrich) was cultured in high glucose (4.5 g/L) DMEM supplemented with 10% hi-FBS (Sigma-Aldrich). The human leukemia monocytic cell line THP-1 (European Collection of Authenticated Cell Cultures, ECACC) was maintained in suspension in RPMI 1640 medium supplemented with 10% hi-FBS (Sigma-Aldrich), 1x non-essential amino acid solution, 1 mM sodium pyruvate and 10 mM HEPES. For *ex vivo* experiments, freshly isolated PBMC from CLD patients were resuspended in RPMI 1640 medium (Sigma-Aldrich) with sodium bicarbonate and L-glutamine, supplemented with 250 μg/mL amphotericin B and 10% hi-FBS. Finally, we employed a model of hepatic macrophages, non-parenchymal cells that consist of embryologically-derived resident ones denominated KC, recruited MDM and capsular macrophages. *Ex vivo* obtained MDM are an appropriate model to study the function of macrophages in hepatic diseases. In order to obtain MDM, freshly isolated PBMC form healthy donors were resuspended in X-VIVO™ 15 culture medium (Lonza) supplemented with 1% hi-FBS, seeded in 6-well plates incubated for 2 h, washed with HBSS and cultured for 5 days in X-VIVO™ 15 supplemented with 1% de hi-FBS and M-CSF 20 ng/mL (Peprotech).

All cell cultures were maintained with 100 U/mL penicillin and 100 μg/mL streptomycin in an incubator (MCO-19AICUV-PE, Panasonic Healthcare Co. Ltd.) at 37ºC, with a humidified 5% CO_2/95% air atmosphere (AirLiquide Medical). Subculturing was performed using 0.25% Trypsin-EDTA and subconfluent cell cultures of passage number lower than 25 were used for all the experiments. Pro-inflammatory or profibrotic stimulation of cells was performed with interferon gamma (IFN-γ) (8 ng/mL), tumor necrosis factor alpha (TNF-α) (12.5 ng/mL), lipopolysaccharide cocktail (LPSc, 50 ng/mL LPS, 12.5 ng/mL IFN-γ and 12.5 ng/mL TNF-α), LPS (2 ng/mL) or TGF-β (2.5 ng/mL).

For the transient transfection experiments in Hep3B cells, Lipofectamine™ 2000 (Invitrogen, Thermo Fisher Scientific) was employed according to the manufacturer's instructions. Cells were seeded in 6-well plates and for the transfection, 100pmol of STAT1 siRNA (Sigma-Aldrich) and 5 μL Lipofectamine™ 2000 were diluted in 250 μL of serum-free Opti-MEM® (Invitrogen, Thermo Fisher Scientific). As a control, SignalSilence® control siRNA (Cell Signaling Technologies) was employed. Diluted siRNA or siControl and Lipofectamine™ 2000 were incubated for 20 min. The transfection mixture (total volume 250 μL) was then added to Hep3B cells (70–80% confluence) in 6-well plates containing 450 μL of Opti-MEM® and incubated for 5 h.

2.5. Isolation of PBMC by density gradient centrifugation

Human PBMC were isolated from peripheral venous whole blood samples obtained from CLD patients using density gradient centrifugation. Briefly, 25 mL were collected in tubes containing sodium citrate as an anticoagulant, diluted with the same amount of PBS and then, layered over Ficoll-Plaque™ medium and centrifuged (400 g, 45 min), thus obtaining PBMC that were then washed with PBS (400 g, 10 min).

2.6. Protein extracts and Western blotting

Total protein extracts from liver samples or cultured cells were obtained, quantified and used for SDS-PAGE as described previously [9]. Primary antibodies included: anti-GAPDH rabbit polyclonal (1:20000, Sigma-Aldrich), anti-STAT3 rabbit monoclonal (1:1000, Cell Signaling Technology), anti-pSTAT3 rabbit monoclonal (1:1000, Cell Signaling Technology), anti-STAT1 rabbit monoclonal (1:1000, Cell Signaling Technology), anti-pSTAT1 mouse monoclonal (1:1000, Abcam), anti--NF-κB (p65) rabbit monoclonal (1:1000, Cell Signaling Technology), anti-pNF-κB (pp65) rabbit monoclonal (1:1000, Cell Signaling Technology), anti-p38 rabbit polyclonal (1:1000, Sigma-Aldrich), anti-pp38 mouse monoclonal (1:1000, Cell Signaling Technology), anti-JNK1/2 rabbit polyclonal (1:1000, Cell Signaling Technology), anti-pJNK1/2 rabbit monoclonal (1:1000, Thermo Fisher Scientific), anti-nucleolin rabbit polyclonal (1:2500, Sigma-Aldrich), anti-CXCL10 mouse monoclonal (1:1000, Abcam), anti-caspase-1 rabbit polyclonal (1:1000, Cell signaling) and anti-NLRP3 rabbit monoclonal (1:1000, Cell signaling). The secondary antibodies were HRP-conjugated anti-rabbit (1:5000, Vector laboratories) and anti-mouse (1:2000, ThermoFisher). Immunolabeling was detected by enhanced chemiluminescence visualized with a digital luminescent image analyser (Amersham), employing Luminata™ Crescendo Western HRP substrate (Merck), or SuperSignal™ West Femto Maximum Sensitivity Substrate (ThermoFisher Scientific). Densitometric analysis was performed using ImageJ software (Fiji). Protein expression is represented as a percentage of control (average expression in the control group was considered 100%), using GAPDH as a loading control.

2.7. Enzyme-linked immunosorbent assay (ELISA)

Hep3B, MDM and LX-2 cells were cultured and treated with RPV. After treatment, cell culture media was recollected and IP-10 (in Hep3B) and MCP-1 (in MDM and LX-2) secretion were measured by ELISA, using a Human CXCL10/IP-10 Quantikine ELISA Kit (R&D Systems Europe) and Human MCP-1 ELISA Kit (Invitrogen) respectively, following the manufacturer's instructions. Briefly, standard (serial dilutions of a recombinant human chemokine) and cell supernatants were added in duplicate to 96-well polystyrene microplates, coated with a monoclonal antibody specific for human IP-10 or MCP-1. Conjugate-HRP was added and plates were incubated (2 h). Following a washing step to remove the excess of conjugate-HRP, a chromogenic substrate solution (3,3',5,5'-tetramethylbenzidine) was added in each well and incubated for 10 min protected from light. The reaction was stopped with stop solution and absorbance was measured at 450 nm with an infinite® 200 PRO series spectrophotometer (TECAN Trading AG). In order to obtain accurate values, background absorbance was also detected at 620 nm and was subtracted from that obtained at 450 nm.

2.8. RNA extraction, cDNA synthesis and quantitative RT-PCR

Extraction and quantification of RNA from liver tissue or cultured cells was performed as described previously [9]. Complementary DNA (cDNA) was synthetized with 1 μg of total RNA using "PrimeScript™ RT Reagent Kit" (Takara Bio). The reaction was performed as suggested in the manufacturer's protocol, in 20 μL final volume and the presence of 4 μL PrimeScript Buffer, 1 μL PrimeScript RT Enzyme Mix I, 1 μL Oligo dT Primer and 1 μL Random 6-mers. The reaction was carried out in SimpliAmp™ Thermal Cycler (Applied Biosystems™) under the following conditions: 37 °C for 15 min, 85 °C for 5 s, 4 °C ∞ . qRT-PCR was performed with SYBR® Premix Ex Taq™ (Tli RNaseH Plus) (Takara Bio), containing TaKaRa Ex Taq HS, dNTP mixture, Mg^{2+}, Tli RNase H and SYBR Green I. The reaction was performed by mixing 1 μL cDNA, 5 μL SYBR® Premix Ex Taq™, 0.2 μM primers (forward and reverse) and RNase-free water (10 μL final volume). qRT-PCR were carried out in a Lightcycler® 96 Real-Time PCR System (Roche Life Science) following this protocol: 95ºC, 30 s; 95ºC, 5 s, 60ºC, 20 s (40 cycles); 95ºC, 1 s; 65ºC, 15 s; 95ºC, 1 s and 40ºC, 30 s). All experiments were performed in duplicate, together with a negative control (RNase-free water instead of cDNA). The primer pairs used (sequences shown in Table 1) were synthetized by Metabion or IDT® (Integrated DNA Technologies). Data were analysed using the comparative CT method, obtaining the relative gene expression of the gene of interest. This method of presenting quantitative gene expression consists in this equation: Fold Change = $2^{-\Delta(\Delta CT)}$, where ΔCT = CT (target gene) - CT (housekeeping gene), and Δ(ΔCT) = ΔCT (treated) - ΔCT (control). *GAPDH* or *ACTB* were used as a housekeeping gene and results were normalized taking into consideration their expression.

2.9. Immunohistochemistry

Mouse liver samples were fixed, embedded in paraffin wax and cut into sections of 5 μm as described previously [9]. Prior to staining, samples were deparaffinized (55ºC for 30 min), rehydrated and rinsed with distilled water. After inducing epitope retrieval with citrate buffer pH.6 antigen retriever (Sigma-Aldrich) (95ºC, 30 min), endogenous peroxidase activity was blocked with 3% hydrogen peroxide solution (Sigma-Aldrich) for 30 min. Slides were subsequently incubated with blocking solution (10% goat normal serum and 1% BSA in TBS, 3 h), anti-CCR2 rabbit monoclonal antibody (Abcam, 1:100, 4ºC, overnight) and SignalStain® Boost Detection Reagent (Cell Signaling, 45 min). The chromogenic substrate peroxidase enzyme 3,3'-diaminobenzidine tetrahydrochloride (DAB Enhanced Liquid Substrate System, Sigma-Aldrich) was employed to immunodetect target antigens. After immunodetection, slides were counterstained with Haematoxylin solution (Gill No. 3; Sigma-Aldrich), dehydrated and mounted with mounting medium (DPX® Mountant for histology, Sigma-Aldrich). Images (10/sample) were acquired using a digital light microscope (Leica DMD 6200, Leica Microsystems) at 40X magnification. Quantifications were performed using the Fiji software.

Table 1
Pairs of primers used for quantitative RT-PCR experiments. Name of the gene, forward and reverse sequences, and size of the amplified products (base pairs) are presented.

GENE	SPECIES	FORWARD PRIMER 5´- 3´	REVERSE PRIMER 5´- 3´	SIZE (bp)
ACTB	human	GGACTTCGAGCAAGAGATGG	AGCACTGTGTTGGCGTACAG	234
ARG1	human	AGGGACAGCCACGAGGAGGG	AGTTTCTCAAGCAGACCAGCCTTTC	70
CCL2	human	AGCAGCAAGTGTCCCAAAGA	GGTTGTGGAGTGAGTGTTCAAG	152
CCL20	human	TTATTGTGGGCTTCACACGG	GGTTCTTTCTGTTCTTGGGCT	212
CCL5	human	ACAGGTCAAGGATGCCAAAGA	GGGTGGGGTAGGATAGTGAG	266
CXCL10	human	GCTGCCTTATCTTTCTGACTCT	TTTTGCTCCCCTCTGGTTTT	290
CXCL9	human	TGTTCTTTTCCTCTTGGGCATC	TGGATAGTCCCTTGGTTGGT	111
CXCR3	human	TGCCTTTGTAGGGGTCAAGT	CTCACAAGCCCGAGTAGGAG	155
GAPDH	human	CTTCTTTTGCGTCGCCAGCC	TTCTCAGCCTTGACGGTGCC	232
IFNG	human	GGCTGAACTGTCGCCAGCAGC	GTTGGCTGCCTAGTTGGCCCC	356
IL10	human	GTGATGCCCCAAGCTGAG	CACGGCCTTGCTCTTGTTTT	138
IL1B	human	TTCGACACATGGGATAACGAGG	TTTTTGCTGTGAGTCCCGGAG	84
IL22	human	GCCCTATATCACCAACCGCA	GCGCTCACTCATACTGACTCC	118
IL6	human	CACTGGTCTTTTGGAGTTTGAGG	ATTTGTGGTTGGGTCAGGGG	169
IL8	human	AGAGACAGCAGAGCACACACAAG	AATTTGGGGTGGAAAGGTTTGG	223
NRLP3	human	AGAACTGTCATCGGGTGGAG	AACTGGAAGTGAGGTGGCTG	174
PPARG	human	GACAGGAAAGACAACAGACAAATC	GGGGTGATGTGTTTGAACTTG	96
SERPINE1	human	CGCTGTCAAGAAGACCCACA	ACCTGCTGAAACACCCTCAC	250
STAT6	human	AGCCCAAGGATGAGGCTTTC	AATCAGGGGCCATTCCAAGG	177
TGFB1	human	CTTCAGCTCCACAAGAAGAACTG	CACGATCATGTTGGACAACTGCTC	297
TLR4	human	CAACCTCCCCTTCTCAACCAA	AGATTTGTCTCCACAGCCACC	264
TNFA	human	AGCCGAATCGCCGTCTCCTA	CAGCGCTGAGTCGGTCACCC	163
Actb	mouse	GCCAACCGTGAAAAGATGACC	GAGGCATACAGGGACAGCAC	95
Adgre1	mouse	TGACTCACCTTGTGGTCCTAA	CTTCCCAGAATCCAGTCTTTCC	111
Ccr2	mouse	CCAGAAGAGGGCATTGGATT	CCAGAAGAGGGCATTGGATT	112

2.10. Migration assay

The monocyte migration assay was performed using the "Calbiochem® Innocyte™ 96-Well Monocyte Cell Migration Assay" kit (Merck Milipore), based on the Boyden chamber principle, which consists of inserting a cell culture coated with a porous membrane into another culture dish. THP-1 cells were washed 2 times with PBS to remove traces of serum and resuspended in non-supplemented X-VIVO™ 15 medium (3×10^6 cells/mL). Then, 150 μL of conditioned medium from MDM treated with RPV for 48 h, human MCP-1 (CCL2) 10 ng/mL in X-VIVO™ 15 medium as a positive control or X-VIVO™ 15 medium without supplementation as a negative control were added to the lower well; all conditions were evaluated in triplicate. 100 μL of the cell suspension were added to the upper well and allowed to migrate for 15 h at 37 °C and 5% CO_2 in a cell incubator. At the end of the migration, media with migrated cells were transferred to a black and conical 96-well plate (provided with the kit), which was centrifuged for 10 min at 300 g. After discarding the supernatant, wells were washed with 200 μL of PBS, and then 100 μL of "Cell Labeling Mixture" (Calcein-AM in PBS) were added to each well. After 30 min of incubation at 37 °C in a CO_2 incubator, fluorescence was detected using a fluorescence plate reader (SpectraMax Gemini XPS, Molecular Devices), with excitation and emission wavelengths of 485 nm and 520 nm, respectively.

2.11. Statistical analysis and presentation of data

All images are representative of at least 3 independent experiments. In most cases, data are represented as % of control, with untreated cells considered 100%. Data are shown as mean±SEM and analysed using GraphPad Prism V.8.01 (GraphPad Software) with unpaired or paired Student's *t*-test (#$p < 0.05$) or a one-way analysis of variance (ANOVA) followed by a Bonferroni test (*$p < 0.05$).

3. Results

3.1. Effect of RPV on stress response pathways

With the aim to better understand the anti-inflammatory effect that RPV showed *in vivo* [9], a targeted transcriptomic analysis was performed in liver samples obtained from a NAFLD mouse model through a comparison between HFD and HFD+RPV mice. During the bioinformatic analysis, a gene set enrichment analysis was performed in order to detect significantly up- or down-regulated blocks of functionally related genes, grouped as biological processes of functions. The results are included in Fig. 1 and consist of the down-regulated GO terms whose adjusted p-value is < 0.005 and are related in the pre-computed GO hierarchies with the following generic GO terms: GO:0006950 (response to stress), GO:0051716 (cellular response to stimulus) and GO:0002376 (immune system process). The analysis revealed 56 down-regulated biological processes in RPV-treated animals that were associated with inflammation, lymphocyte activation, regulation of MAPK cascade, and cell migration, hence we decided to delve more deeply into these processes. Firstly, given that several GO terms referred to regulation of stress-activated MAPK (GO:0032874, GO: 0070304 and GO:0043405), we assessed the presence of phosphorylated (activated) JNK and p38 in whole liver tissue through WB, and observed that HFD led to an increase in both parameters which was significantly reversed in the HFD+RPV group (Fig. 2A). Secondly, our aim was to address the stress response in the major hepatic cell populations by assessing these signaling pathways upon exposure to RPV under basal conditions or submitted to pro-inflammatory stimuli and co-treated with RPV. In Hep3B cells exposed to LPSc, we observed a tendency towards activation of p38 and JNK (increased levels of pp38 and pJNK) which was reversed by co-treatment with RPV (Fig. 2B). In the case of the HSC cell line LX-2, stimulation with the profibrotic cytokine TGF-β lead to an increase in the levels of the phosphorylated form of JNK, but not that of p38 (Fig. 2C). Moreover, RPV diminished the amount of pp38 in the control (unstimulated cells), while there was no effect in TGF-β exposed cells. Regarding pJNK, RPV displayed a tendency to reverse the increase induced by TGF-β. Finally, in human MDM, RPV reduced the levels of both pJNK and pp38 in a concentration-dependent fashion (Fig. 2D). It is noteworthy that in MDM, both the levels of pp38 and those of pJNK1 were enhanced by the treatment with vehicle (DMSO).

3.2. Anti-inflammatory and immunomodulating effect of RPV

The capacity of RPV to exert anti-inflammatory and immunomodulating effects was assessed in several models. Firstly, the transcriptomic

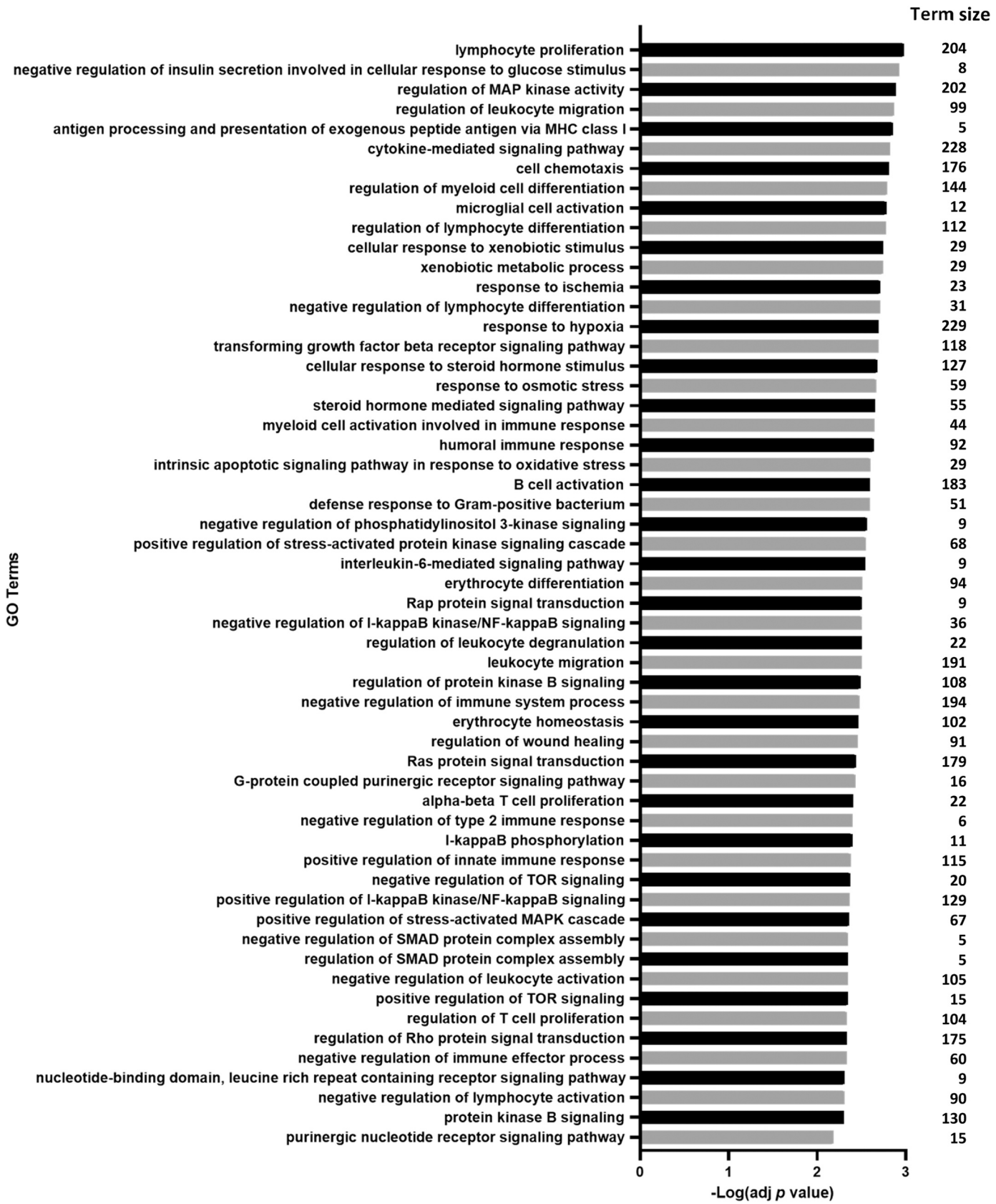

Fig. 1. List of biological functions related to inflammation and leukocyte chemotaxis/migration that are significantly downregulated in rilpivirine-treated HFD-fed mice**.** The terms "Gene Ontology" (GO) are shown. Data were obtained from gene set enrichment bioinformatics analysis performed after transcriptomic RNA analysis of whole liver tissue from mice in the HFD and HFD+RPV groups (n = 3). Adjusted p-value < 0.005.

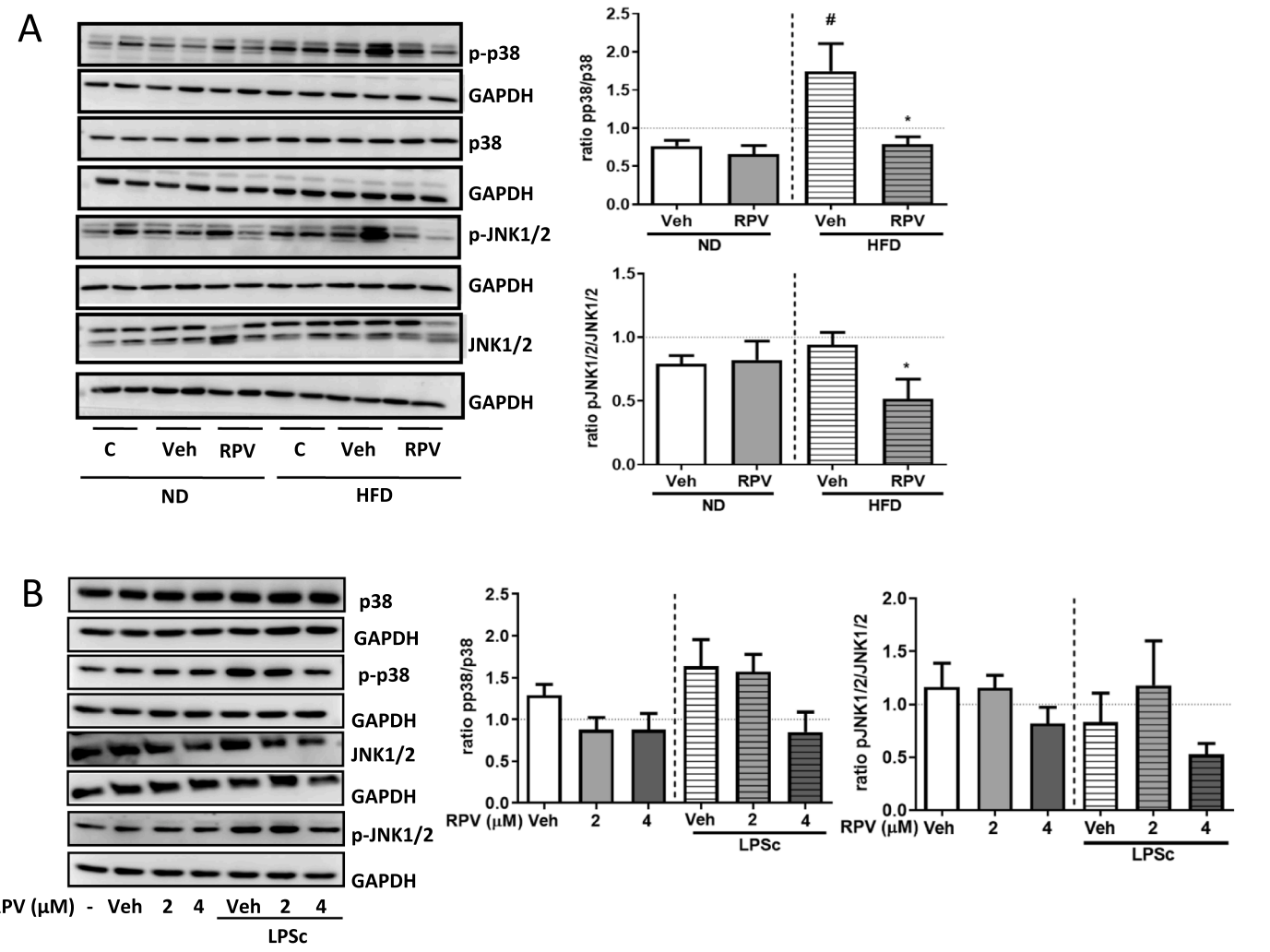

(caption on next page)

Fig. 2. Effect of rilpivirine on the activation of stress kinases in the liver of NAFLD mouse model and *in vitro*, in two human hepatic cell types (Hep3B and LX-2) and human MDM. Western blot analyses of p38, JNK and their phosphorylated forms pp38 and pJNK are shown with representative images and densitometric quantification, expressed as ratio between the phosphorylated and the total amount of the protein, being the ratio in the untreated cells (Control) considered 1. Results include (A) Whole-liver samples of a mouse model of NAFLD exposed to vehicle or RPV (mean±SEM, n = 7–8); (B) Hep3B cells unstimulated or stimulated with LPSc for 24 h and then RPV added for additional 24 h without refreshing the medium (mean±SEM, n = 4–9). (C) LX-2 cells exposed to increasing concentrations of RPV alone or co-treated with TGF-β + RPV for 48 h (mean±SEM, n = 3–4). (D) MDM treated with a range of increasing concentrations of RPV for 48 h (mean±SEM, n = 3–4). Data, normalized vs those of the reference protein GAPDH, were statistically analysed by one-way ANOVA with Bonferroni post-test (**p < 0.01, RPV vs. Veh in C) or with Student's t-test (*p < 0.05, RPV vs. Veh in A and #p < 0.05 Veh-HFD vs Veh-ND in A). ND, normal diet; HFD, high fat diet.

analysis revealed alterations of IκB/NF-κB signaling in whole liver samples of HFD mice treated with RPV compared to HFD mice (GO:0007252, GO:0043123 and GO:0043124), as shown in Fig. 1. When Hep3B cells were treated with TNF-α as a stimulus for NF-κB activation, we observed increased nuclear presence of p65, which was slightly diminished with co-treatment with RPV (Fig. 3A). In the case of LX-2 cells, treatment with TGF-β did not significantly alter p65 signaling (data not shown). Also, no significant effect of RPV on the activation of this transcription factor was observed in neither LX-2 cells nor MDM (data not shown).

Given the role of inflammasomes in the inflammatory process, we studied the activation of NLRP3 inflammasome whose assembly leads to caspase-1-dependent release of the pro-inflammatory cytokines IL-1β and IL-18. In LX-2 cells exposed to TGF-β, activation of caspase-1 (cleavage of procaspase-1 to produce caspase-1) was enhanced and co-treatment with RPV, in a concentration-dependent manner, showed a tendency to normalize this activation (Fig. 3B). Interestingly, RPV actually led to a decrease in caspase-1 activation even under basal conditions (without TGF-β). Similarly, in MDM, RPV diminished the protein levels of NLRP3, activated caspase-1 and pSTAT1, a major pro-inflammatory transcription factor in leukocytes (Fig. 3C). In addition, in these cells, RPV stimulated anti-inflammatory signaling through enhanced gene expression of *STAT6* and its targets *PPARG* and *ARG1* (Fig. 3D). Furthermore, we observed a positive and significant correlation between *STAT6* expression and that of *PPARG* and *ARG1* in RPV-treated MDM enforcing the idea of RPV triggering one of the most vital anti-inflammatory axes in leukocytes, STAT6-PPARγ-ARG1 (Fig. 3E). Finally, we also aimed to analyze the capacity of RPV to exert anti-inflammatory actions under pro-inflammatory conditions. For this, MDM were exposed to LPS as a pro-inflammatory stimulus and co-treated with RPV, and mRNA levels of several inflammation markers were studied (*IL18*, *IL6*, *IL8* and *NLRP3*). Of note, the gene expression of all these markers was enhanced with LPS while RPV rescued this increase in a concentration-dependent manner (Fig. 3F). Altogether, these findings point to an anti-inflammatory action of RPV in MDM, both under basal and inflammatory conditions.

3.3. Effect of RPV on leukocyte migration and recruitment

The transcriptomic analysis revealed downregulation of several GO terms associated with leukocyte migration in whole liver samples of HFD+RPV mice compared to HFD (GO:0002685, GO:0050900 and GO:0060326) (Fig. 1). In order to delve into this process more deeply, we assessed the presence/recruitment of macrophages in the liver of HFD vs ND mice and RPV's effect on it. qRT-PCR analysis using whole liver samples of *Adgre1* (F4/80), a classical marker of mature macrophages, revealed a slight increase in HFD vs ND mice. Of note, RPV produced a major decrease of *Adgre1* expression in both ND and HFD mice (Fig. 4A). We also analyzed the mRNA levels of *Ccr2*, as a crucial receptor in the liver for monocyte/macrophage recruitment, and observed that they were upregulated in HFD mice while RPV rescued this effect (Fig. 4B). This result was corroborated through immunohistochemistry of liver sections (Fig. 4C), observing that chronic administration of RPV decreased the number of CCR2 + cells in the periportal area in this murine model of NAFLD. aHSC secrete many immunomodulatory cytokines and chemokines to regulate the phenotype and function of monocytes, NK cells and T cells, including CCL2. With this in mind, we studied the production of CCL2 by LX-2 cells and human MDM, assessed as mRNA levels (qRT-PCR) and secretion of this chemokine in the extracellular medium (ELISA). Importantly, in both unstimulated and TGF-β-treated LX-2 cells RPV led to a decrease in the intracellular and secreted levels of CCL2 (Fig. 4D,E). A very similar result was obtained with MDM exposed to RPV (Fig. 4F,G). In addition, RPV diminished *CCL2* gene expression in MDM under pro-inflammatory conditions (LPS) in a concentration-dependent manner (Fig. 4H). To further delve into the capacity of RPV to interfere with chemotaxis, a migration assay was performed in which THP-1 cells (human monocytic cell line) were left to migrate towards conditioned medium obtained by treatment of MDM with RPV. Although no statistically significant results were obtained, RPV showed a clear tendency to reduce the number of migrated cells (Fig. 4I).

Beside CCL2/CCR2 axis, CXCL10/IP-10 is a pivotal recruiter of immune cells, especially leukocytes, to the liver parenchyma and a key inflammatory mediator in NASH [14]; therefore, we next analysed CXCL10/IP-10 protein levels in the same mouse model (Fig. 5A). There was no significant increase of CXCL10/IP-10 expression in the livers of the animals fed with HFD compared to those with ND, however RPV significantly reduced CXCL10/IP-10 protein expression in the HFD+RPV group. Given the fact that one of the most prominent targets of STAT1 regulation is CXCL10/IP-10, we hypothesized that part of the hepatoprotective effects of RPV are related to downregulation of STAT1 and the consequently decreased CXCL10/IP-10 expression in hepatocytes. RPV significantly reduced mRNA expression of CXCL10/IP10 (Fig. 5B), as well as its extracellular levels studied by ELISA (Fig. 5C), in Hep3B cells. In order to evaluate if reduced CXCL10/IP10 expression depends directly on STAT1 activation, we transiently silenced STAT1 in Hep3B by means of RNA interference (Fig. 5D). Interestingly, it was observed that *STAT1* silencing led to an increase in *CXCL10* expression in Hep3B, while RPV's effect on *CXCL10* expression was preserved (Fig. 5E). Additionally, Hep3B cells were treated with the chemical inhibitor of STAT1, fludarabine (5 μM), and similar results were obtained as fludarabine enhanced *CXCL10* gene expression, while once again RPV induced its down-regulation (Supplementary Fig. 1). These findings suggest that transcription factors other than STAT1 are involved in the effect of RPV on *CXCL10* expression. Regarding MDM treated with RPV, we detected no changes in *CXCL10* expression (data not shown).

3.4. Anti-inflammatory effect of RPV ex vivo in PBMC isolated from patients with CLD

The characteristics of the 38 study participants are shown in Table 2. Regarding the etiology of CLD, the majority of patients had suffered from or presented HCV infection (34.2%), followed by those with persistent alcohol consumption (21.5%) and patients within the mixed etiology group (21.5%), meaning that they were affected at the same time by at least two chronic liver conditions. Seven patients were diagnosed with NASH, one was HBV-infected, and no data were available for another patient. As for the presence of metabolic comorbidities, 34.2% had arterial hypertension, 36.8% were diabetic and 14 of them suffered from dyslipidemia. The data about LF detected by FibroScan®, ultrasound-based transient elastography that measures liver stiffness (elasticity), showed that 39.5% had the lowest grade, F0-F1, while 23.7% were F2 and 31.6% had the most severe (F3-F4 grade). Liver stiffness is normally between 2 and 6 kPa and in the present cohort the

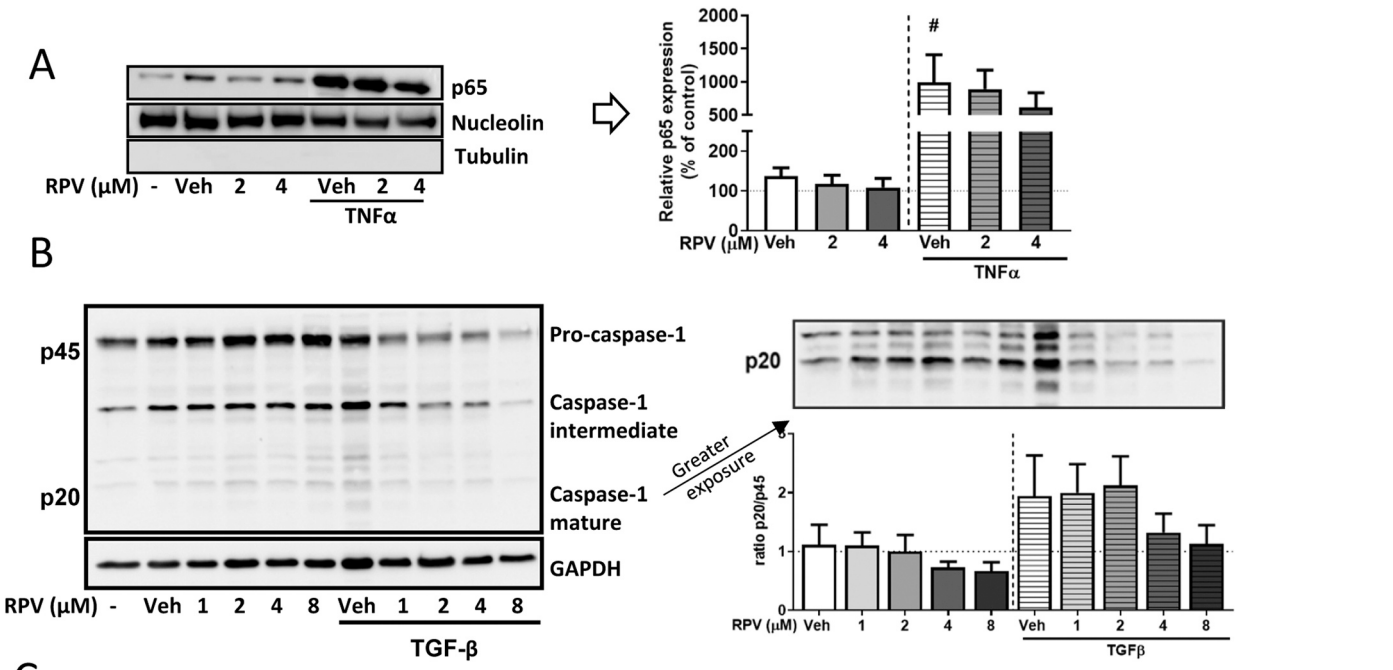

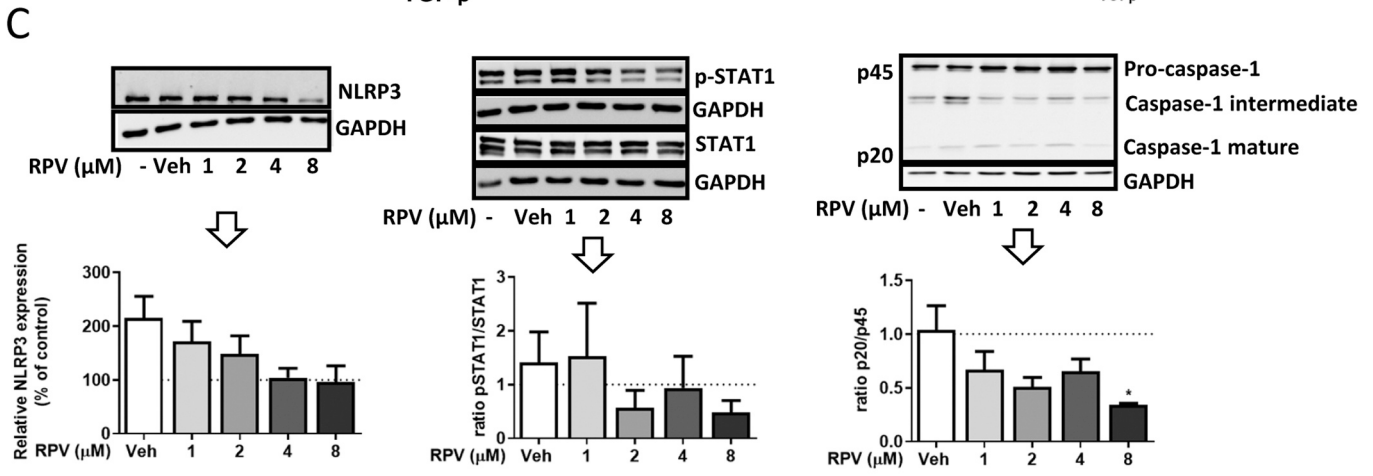

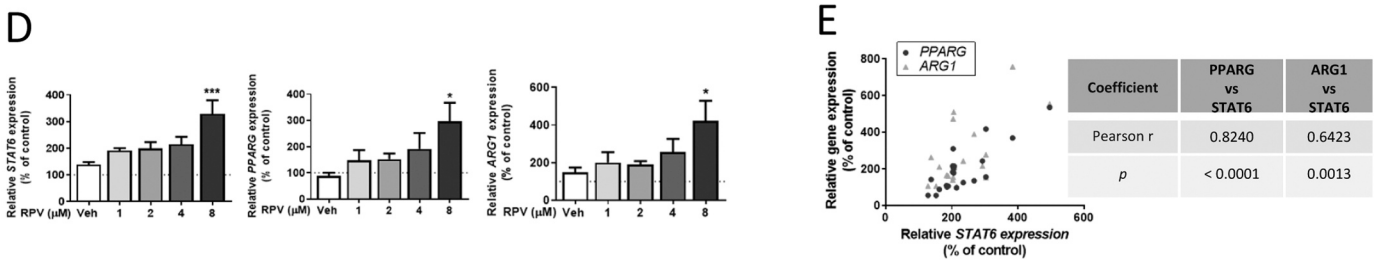

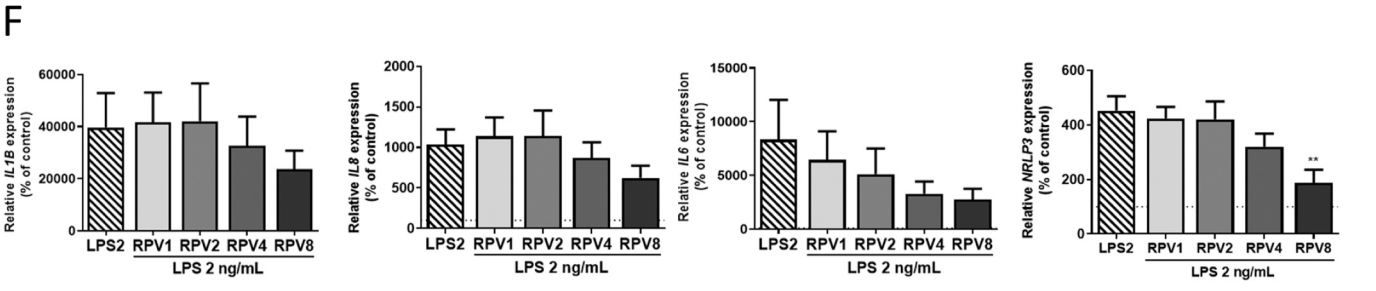

(caption on next page)

Fig. 3. Effect of rilpivirine on several markers of inflammation (NF-κB, NLRP3 inflammasome and STAT activation) in Hep3B, LX-2 and MDM. For all western blot analysis, representative images and densitometry data are shown. (A) Hep3B cells were pre-treated with 12.5 ng/mL TNF-α for 24 h and RPV or Veh (DMSO) were added for another 24 h. Western blot analysis of nuclear p65 levels was performed and data were normalized vs the housekeeping protein nucleolin (mean±SEM, n = 4–8). (B) LX-2 cells were exposed to increasing concentrations of RPV or co-treated with TGF-β + RPV or Veh (DMSO) for 48 h. Representative WB images of caspase-1 levels; activation of caspase-1 was evaluated by means of the ratio between the active form, of 20 kDa, and the pro-caspase-1, of 45 kDa (mean±SEM; n = 3–5). (C) MDM were treated with increasing concentrations of RPV for 48 h. Representative WB images of NLRP3, STAT1 and caspase-1 levels. Quantification of STAT1 activation was performed as ratio between the phosphorylated form and the total form of the protein (mean±SEM; n = 3–5). All results are represented as relative expression with respect to that observed in untreated cells (control, considered 100% or 1, in the ratio). Statistical analysis was performed using the one-way ANOVA test, followed by a Bonferroni test, *p < 0.05 for the treatment with RPV compared to its vehicle. Comparison of Veh-TNFα vs Veh was performed with Student's t-test (#p < 0.05). In B and C, protein expression was normalized against the expression of the reference protein GAPDH. (D,E) Study of STAT6/PPARG/ARG1 pathway. mRNA levels of *STAT6*, *PPARG* and *ARG1* and correlation between *STAT6* and *PPARG* and with *ARG1* are shown (r: Pearson's correlation coefficient). Results (mean±SEM; n = 5–6) are represented as relative expression to that observed in untreated cells (control, considered 100%) and normalized against *ACTB* expression. Statistical analysis was performed using the one-way ANOVA test, followed by a Bonferroni test (*p < 0.05 and ***p < 0.001 in the case of treatment with RPV compared to its vehicle). (F) Gene expression study by RT-qPCR of inflammatory mediators in MDM stimulated with LPS (2 ng/mL) for 1 h and further co-treated with different concentrations of RPV for 48 h. The results (mean±SEM; n = 4–7) are represented as relative expression with respect to that observed in untreated cells (control, considered 100%). Gene expression data were normalized against *ACTB* expression. Statistical analysis was performed using the one-way ANOVA test, followed by a Bonferroni test (**p < 0.01) for RPV treatment with respect to the pro-inflammatory stimulus alone (LPS).

median value of LS was above the normal range. Controlled attenuation parameter (CAP) quantifies liver steatosis and is measured as ultrasound attenuation. Normal values range from 100 to 400 dB/m; in this cohort, the median value was 278 dB/m. 17 patients had cirrhosis (compensated in 11 patients and decompensated in 6). Regarding the biochemical and hematological parameters of all the patients, all median values were within the range considered normal, except for ferritin and GGT levels, whose values were above the upper limit of the normal range. The analysis of hematological, biochemical and markers of liver function in the patients with CLD classified according to the etiology of their liver pathology and as a comparison between patients with fibrosis F0-F1 and F4 are shown in Supplementary Fig. 2 and 3 respectively. In order to analyze whether RPV can also exert anti-inflammatory effects in patients with CLD, we treated PBMC isolated from these CLD patients with clinically relevant concentrations of RPV (1 and 4 μM) *ex vivo* for 24 h. We studied the gene expression of several chemokines including CXCL10 and its receptors CXCR3 and TLR4, CXCL9, CCL2 and CCL20, in addition to several pro-inflammatory, profibrotic and anti-inflammatory markers (Fig. 6A). A concentration-dependent decrease in *CXCL10* and *CXCL9* mRNA levels was observed, with no change in their receptor *CXCR3*. Another altered mediator was the pro-inflammatory and profibrotic marker *SERPINE1*, whose expression was downregulated with RPV (Fig. 6A). Finally, a concentration-dependent tendency for an increase in the expression of anti-inflammatory mediators was observed in *IL-22* and *IL-10* (statistically significant) (Fig. 6B). Also, RPV led to a significant and concentration-dependent decrease in the levels of pSTAT1, while no changes in pSTAT3 and a tendency for increased IκB were detected (Fig. 6C).

4. Discussion

The worldwide prevalence of CLD and, particularly that of its more frequent form NAFLD is increasing dramatically. Multiple drugs have been used to combat different manifestations and risk factors associated with CLD, but there is a lack of specific pharmacological agents to target it. More significantly, there is absence of approved anti-fibrotic compounds and with this, pharmacological repurposing has gained special interest. Beyond its well-described role in combined antiretroviral therapy, RPV has shown a clear anti-inflammatory effect in different preclinical models of CLD [9]. The present study has associated this effect with its actions on different cell types in multiple experimental settings.

The chemokine system is critical for the function of the immune system as it organizes the migration and localization of immune cells in different tissues by the exertion of chemotactic effects. In recent years, extensive *in vivo* and *in vitro* studies have shown that CCR2, a chemokine receptor primarily expressed on the surface of monocytes/macrophages and lymphocytes, and its ligand system play a fundamental role in liver pathology [15]. CCR2 drives the pathogenesis of acute liver injury and CLD, through its role in inflammation, LF and tumor progression. In addition, both preclinical and phase IIb studies have shown that the dual CCR2/CCR5 antagonist cenicriviroc is an effective and safe anti-fibrotic agent for treating alcohol-induced steatohepatitis and NASH [16,17]. However, it is important to note that the AURORA Phase III randomized study did not demonstrate the efficacy of cenicriviroc for treating LF assessed by histology in adults with NASH [18]. Our data show that mice exposed to HFD and RPV display less CCR2 expression in the liver compared to HFD, and both MDM of human origin and LX-2 cells secrete less CCL2 if treated with RPV in a concentration-dependent manner. Importantly, PBMC of patients with CLD exposed to RPV also display diminished expression of CCL2. This is in line with RPV diminishing the capacity of monocytes to migrate shown *in vitro* and also with the fact that the livers of HFD+RPV mice show smaller presence of macrophages compared to mice exposed only to HFD.

One particularly important pro-inflammatory cytokine associated with lipotoxicity is CXCL10/IP-10, which recruits inflammatory cells (monocytes, macrophages and T cells) to the site of damaged/inflamed liver tissue. In various types of liver injury, CXCL10 is secreted by hepatocytes in areas of lobular inflammation [19,20]. Moreover, CXCL10 has been associated with NASH, as it is upregulated in patients [21] and circulating CXCL10 levels is an independent risk factor for patients with NASH [14]. Overall, CXCL10 could be viewed as a pivotal molecule that facilitates transition from benign steatosis to progressive hepatocellular damage, inflammation and fibrosis in this condition. In our mouse model of NAFLD, whole liver tissue displayed only a slight increase in IP-10 expression, however treatment with RPV significantly diminished it. This result was supported by *in vitro* data of RPV downregulating both basal and IFN-γ-induced CXCL10/IP-10 expression. However, this effect was not mediated by STAT1, one of the pivotal regulators of *CXCL10* transcription, suggesting the involvement of other, non-canonical IFN pathways in such effect, being the main ones the MAP kinases and the phosphoinositide 3-kinases (PI3K)/mammalian target of rapamycin (mTOR) pathways. RPV also dramatically reduced *CXCL10* mRNA levels in PBMC of patients with CLD treated *ex vivo*.

In addition, our findings reveal that the anti-inflammatory action of RPV is a common theme among the different cell types in the liver. RPV downregulates p38 and JNK, also known as the stress-activated protein kinases (SAPK), which are essential for the production of the pro-inflammatory mediators TNF-), IL-6, IL-1 and IL-8, as well as for activation of transcription factors NF-κB, AP1, and hypoxia-inducible factor 1 (HIF-1). JNK and p38 signaling pathways also trigger the secretion of cytokines and chemokines, leading to the recruitment of monocytes,

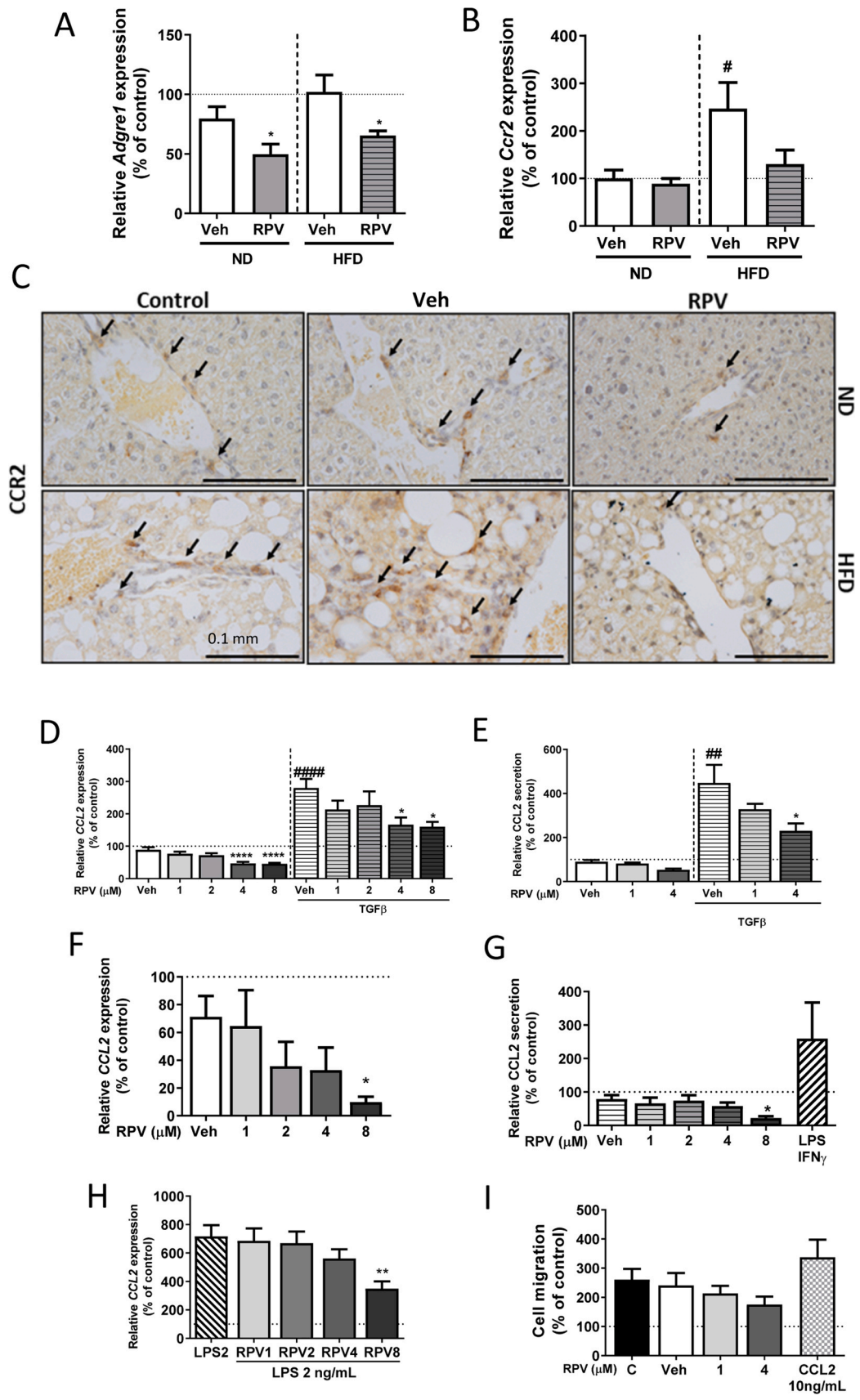

Fig. 4. Effect of rilpivirine on the hepatic infiltration of macrophages in a NAFLD mouse model and on CCL2 levels *in vivo* and *in vitro*. Gene expression analysis by qRT-PCR of (A) the macrophage marker *Adgre1* (F4/80), and of (B) *Ccr2*, characteristic of infiltrated macrophages, in liver tissue of mouse model of NAFLD. Data (mean ±SEM; n = 6) are represented as relative expression with respect to that observed in untreated mice of the ND group (control, considered 100%). Gene expression data were normalized against *Actb* expression. Statistical analysis: Student's t-test (*$p < 0.05$, RPV vs. Veh and #$p < 0.05$, Veh ND vs. Veh HFD). ND, normal diet; HFD, high fat diet. (C) Representative IHC images of CCR2 in the periportal area of the liver (n = 4). Black arrows point to positive cells. Scale bar= 0.1 mm. (D,E) LX-2 cells were treated with TGF-β alone or in the presence of increasing concentrations of RPV for 48 h. *CCL2* mRNA levels were studied by qRT-PCR (D) and extracellular secretion of CCL2 was assessed by ELISA (E). Results (mean±SEM; n=4–6) are represented as relative levels to that observed in untreated cells (control, considered 100%); mRNA levels were normalized against *ACTB* expression. (F,G) MDM were treated with increasing concentrations of RPV for 48 h, and mRNA levels of *CCL2* were assessed by RT-qPCR (F) and secreted CCL2 was studied by ELISA (G). The results are shown as mean±SEM of n = 5–6 (F) and n = 4 (G) of relative expression/secretion with respect to that observed in untreated cells (control, considered 100%); mRNA levels were normalized against *ACTB* expression. (H) Gene expression study by RT-qPCR of *CCL2* in MDM stimulated with LPS (2 ng/mL) for 1 h and further co-treated with different concentrations of RPV for 48 h. The results (mean±SEM; n = 5) are represented as relative expression with respect to that observed in untreated cells (control, considered 100%); data were normalized against *ACTB* expression. (I) THP-1 cell migration test towards conditioned medium of MDM treated with different concentrations of RPV for 48 h. Results (mean ±SEM; n = 4) are represented as relative migration with respect to that observed towards medium without serum (control, considered 100%). Positive control: LPS (0.1 μg/mL) + IFN-γ (20 ng/mL) (G) or CCL2 (10 ng/mL (I). Statistical analysis was performed using the one-way ANOVA test, followed by a Bonferroni test (*$p < 0.05$, **$p < 0.01$, ****$p < 0.0001$) for treatment with RPV compared to its vehicle (D,E,F,G,I) or LPS treatment alone (H), or Student's t-test for the treatment of TGF-β vs Vehicle (##$p < 0.01$, ####$p < 0.0001$).

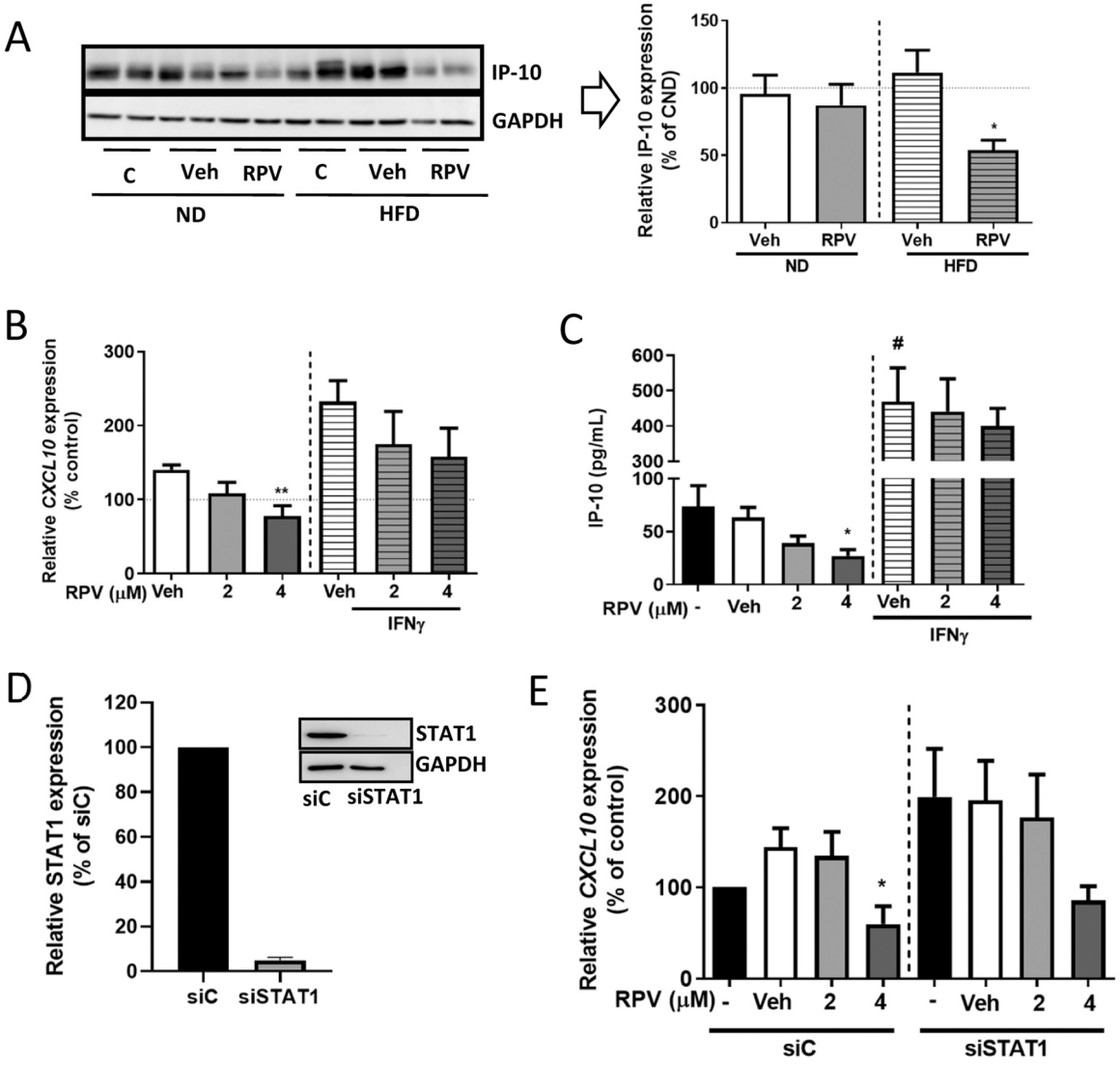

Fig. 5. Effect of rilpivirine on CXCL10 (IP-10) levels *in vivo* (in a NAFLD mouse model) and *in vitro*. (A) Western blot analysis of IP-10 - densitometry and representative images are shown. Data (mean±SEM, n = 7–8) were normalised vs those of the reference protein GAPDH. Statistical analysis: Student's t-test: *p < 0.05 RPV vs. Veh. ND, normal diet; HFD, high fat diet. (B.C,D,E) Effect of RPV on CXCL10 in Hep3B cells. Cells were pre-treated with IFN-γ (8 ng/mL) for 24 h and RPV (2 or 4 μM) or Veh (DMSO) were added for additional 24 h. (B). qRT-PCR analysis of CXCL10 mRNA levels (n = 6–8). (C). Levels of secreted CXCL10 measured by ELISA (n = 2–4). Data (mean±SEM) are expressed as percentage of untreated cell (control) which was considered 100% and were analysed by one-way ANOVA with Bonferroni post-test, *p < 0.05, * *p < 0.01 vs Veh, or Student's t test #p < 0.05 Veh vs IFN-γ + Veh. (D,E). RPV's effect on CXCL10 expression in Hep3B cells lacking active STAT1. The expression of CXCL10 in siControl cells was considered 100% (D). RT-qPCR analysis of *CXCL10* (n = 4) after transient transfection with siC or siSTAT1 (E). Analysis of the protein levels of STAT1 by WB - densitometry and a representative image are shown (n = 3). Data were normalised vs those of the reference protein GAPDH and were analysed by one-way ANOVA with Bonferroni post-test *p < 0.05 vs Veh.

neutrophils, and various types of lymphocytes. The fact that RPV clearly downregulates these pathways *in vivo* and *in vitro* is of particular interest, as understanding the mechanisms by which immune cells are activated and recruited to the liver is considered paramount for the detection of novel targets for the treatment of liver diseases. The therapeutic potential of JNK inhibitors has been shown in preclinical studies of liver diseases, including acute liver failure, ischemia/reperfusion injury, LF, HCC, NAFLD and NASH [22]. Nevertheless, to our knowledge there have not been SAPK inhibitors in clinical trials for the treatment of CLD due to their non-specificity and side effects.

The STAT family of transcription factors includes seven members that are activated in response to different cytokine-receptor interactions. In this study, we provide evidence of the capacity of RPV to interfere with the activation of some of these factors in the context of CLD. In immune cells such as leukocytes and macrophages, STAT1 activates the inflammatory response, while STAT6 is involved in the resolution of inflammation by inducing the development of Th2 lymphocytes and M2-type macrophages. In the same context, STAT6 promotes the activation of PPARγ which, besides being a major regulator of fatty acid synthesis and storage, and glucose metabolism, exerts anti-inflammatory properties [23]. Here, we provide evidence that MDM exposed to RPV display diminished STAT1 activation in parallel with an increase in the expression of *STAT6*, *PPARG* and *ARG1*. Treatment with RPV also led to a decrease in pSTAT1 levels in PBMC from patients with CLD.

The present study offers clues for the hepatoprotective effect of RPV in a mouse model of NAFLD. The customized diet employed (59% fat plus 2% free cholesterol for 12 wks) led to a significant development of steatohepatitis with fibrosis, as revealed by multiple molecular and histological markers [9]. This is also supported by abundant literature which shows that in preclinical models, cholesterol-containing HFD rather than HFD diet alone confers features similar to clinical NASH including hepatic inflammation and fibrosis [24–27].

Table 2
Characteristics of the patients with chronic liver disease. Variables include general characteristics (anthropometry and substance abuse), disease etiology, comorbidities-related parameters, and liver fibrosis-related parameters. Data from general biochemical and hematological analyses are also included. Values are expressed as number of patients and percentage of total number of patients for non-numerical data, and median (1st and 3rd percentiles) for numerical data. ALT, alanine aminotransferase; ALP, alkaline phosphatase; AST, aspartate aminotransferase; BMI, body mass index; CAP, controlled attenuation parameter; CRP, C-reactive protein; GGT, gammaglutamyl transferase; INR, international normalized ratio; Hg, hemoglobin; HBV, hepatitis virus B; HCV, hepatitis virus C; HDL, high density lipoprotein cholesterol; LDL, low density lipoprotein cholesterol; TC, total cholesterol, TG, triglycerides.

GENERAL CHARACTERISTICS OF THE PATIENTS						
GENDER	**MALE**	**FEMALE**				
	28 (72.5%)	10 (27.5%)				
AGE (years) median (IQR)	58.5 (55.0 – 68.3)					
BMI (kg/m^2) median (IQR)	26.5 (24 – 31)					
SMOKING	YES	NO	PREVIOUS SMOKER			
	8 (21.1%)	22 (57.9%)	8 (21.1%)			
ALCOHOL USE	YES	NO	PREVIOUS			
	9 (23.7%)	23 (60.5%)	6 (15.8%)			
COMORBIDITIES-RELATED PARAMETERS						
ARTERIAL HYPERTENSION	YES	NO				
	13 (34.2%)	25 (65.8%)				
DIABETES MELLITUS	YES	NO				
	14 (36.8%)	24 (63.2%)				
DYSLIPIDEMIA	YES	NO				
	14 (36.8%)	24 (63.2%)				
ETIOLOGY	NASH	ALCOHOL	HCV	HBV	MIX	OTHER
	7 (18.4%)	8 (21.5%)	13 (34.2%)	1 (2.6%)	8 (21.5%)	1 (2.6%)
FIBROSIS-RELATED PARAMETERS						
LIVER FIBROSIS (grade)	F0-F1	F2	F3-F4	NO DATA		
	15 (39.5%)	9 (23.7%)	12 (31.6%)	2 (5.3%)		
ELASTICITY (kPa) median (IQR)	7.80 (5.45 – 11.35)					
CAP (dB/m) median (IQR)	278 (212.8 – 305)					
HEPATIC CIRRHOSIS	COMPENSATED	DECOMPENSATED	NO			
	11 (28.9%)	6 (15.8%)	21 (55.3%)			
BIOCHEMICAL ANALYSIS			HEMATOLOGICAL ANALYSIS			
PARAMETER	VALUE (IQR)	REFERENCE	PARAMETER	VALUE (IQR)	REFERENCE	
Glucose (mg/dL)	104.5 (93–136.8)	64–106	Leukocytes * 10^9/L	5.46 (4.9 – 7.9)	3.9–11	
Urea (mg/dL)	38.5 (31.3 – 47.5)	20–50	Neutrophils * 10^9/L	3.1 (2.2–4.5)	2.5–7.5	
Creatinine (mg/dL)	0.8 (0.7–1)	0.51–0.95	Lymphocytes * 10^9/L	1.7 (1.3–2.4)	1.5–4.5	
Ferritin (ng/mL)	128 (65.3 – 226)	10–120	Monocytes * 10^9/L	0.5 (0.4–0.7)	0.2–0.8	
Total cholesterol (mg/dL)	175.5 (155 – 204.3)	140–200	Eosinophils * 10^9/L	0.1 (0.1–0.25)	0.05–0.5	
HDL cholesterol (mg/dL)	51 (46–63.5)	> 35	Basophils * 10^9/L	0.04 (0.02–0.06)	0.01–0.15	
LDL calculated (mg/dL)	109.5 (93.3–133.8)	< 130	Platelets * 10^9/L	176 (112.8 – 253.5)	140–400	
TG (mg/dL)	89 (75.3 – 131.8)	40–160				
ALT (U/L)	31 (18.3 – 56.8)	1–31				
AST (U/L)	32 (27–45.5)	1–31				
GGT (U/L)	67 (31 – 101.8)	1–38				
ALP (mU/mL)	85 (64.3 – 102.5)	30–120				
Hg (g/dL)	14.4 (13.5–15.9)	11.2–15.5				
Bilirubin (mg/dL)	0.6 (0.5–0.8)	0.1–1.0				
Albumin (g/dL)	4.4 (4.2–4.6)	3.5–5.2				
INR	1.04 (1–1.1)	0.85–1.35				
CRP (mg/L)	2.1 (1.1–4)	0–5				

An obvious limitation of our study is the use of only female mice in the animal model of liver injury. We employed C57BL/6 J mice, one of the most commonly used mouse strains in experimental research of metabolic diseases. Both male and female C57BL/6 J mice are highly sensitive to obesogenic stimuli and the development of NAFLD, and several reports even indicate higher levels of liver injury in females in different NAFLD models. In one study, female C57BL/6 J mice with NAFLD (induced by adding 30% fructose solution in the drinking water for 16 wks) showed markedly more pronounced liver inflammation compared to male mice, while hepatic steatosis was similar [28]. Similarly, in another study, while WT C57BL/6 J mice displayed only steatosis after a short-term high fat+cholesterol diet, both male and female ldlr(-/-)/ APOE2ki mice showed severe liver inflammation, but marked steatosis was only present in females [29].

Besides the fact that hormonal levels/fluctuation in females may modulate some aspects of nutritional models of NAFLD, gender differences have been especially associated with differences in body weight and, in some cases, with the development of advanced NASH [30,31]. In our model, we did observe a significant development of steatohepatitis with LF in female C57BL/6 J mice and thus the finding that RPV is hepatoprotective in this model is relevant.

In conclusion, we provide evidence of anti-inflammatory and immunomodulating actions of RPV in the context of CLD using different *in vivo*, *ex vivo* and *in vitro* models. These findings shed light on the mechanisms involved in the hepatoprotective effects of RPV and may be helpful in the search for novel drugs, novel druggable targets and drug repositioning strategies for the therapeutics of CLD.

Funding

This research was funded by the Instituto de Salud Carlos III (CIBER CB06/04/0071 -co-funded by the European Regional Development Fund of the European Union-), Generalitat Valenciana (AICO2021/017 and CIPROM/2021/044), FISABIO (UGP-21-236) and PID2021-127945OB-I00 from the Spanish Ministry of Science and Innovation (MCIN/AEI/10.13039/501100011033, co-funded by the European Regional Development Fund of the European Union- A way to make Europe A.B.M and I.F.M are the recipients of Predoctoral Trainee

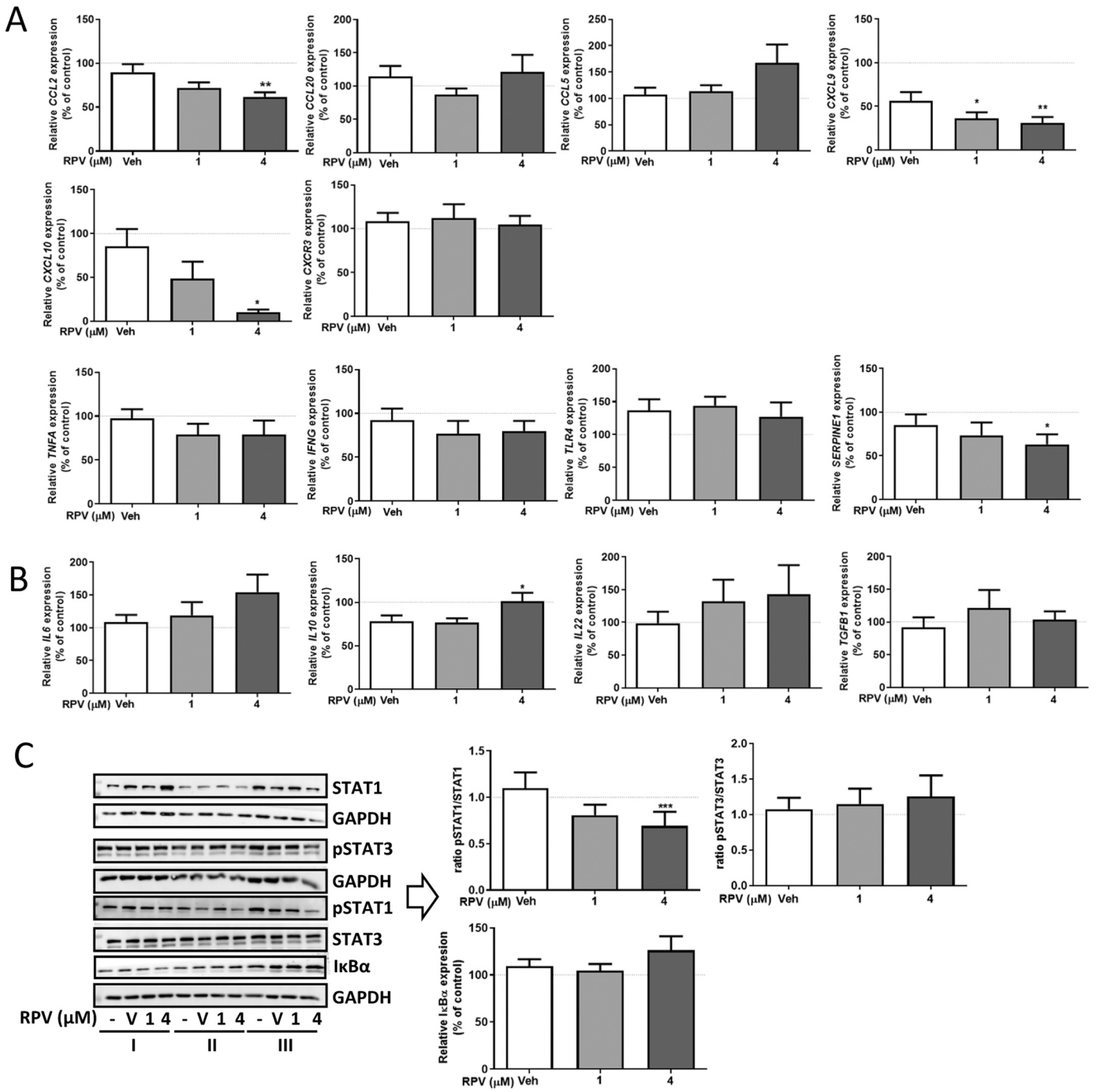

Fig. 6. Expression of selected inflammation and immunoregulatory markers in PBMC isolated from CLD patients after treatment with RPV *ex vivo*. (A) Relative mRNA levels of chemokines, chemokine receptors and other pro-inflammatory mediators. (B) Relative mRNA levels of anti-inflammatory mediators. (C) Western blot analysis of STAT1, pSTAT1, STAT3, pSTAT3 and IκBα in whole-cell protein extracts. Cells were treated for 24 h with RPV (1 and 4 μM), vehicle (DMSO) or left untreated (control) (n = 13–17). Relative mRNA expression was analyzed by RT-qPCR. In the western blot analysis, graphical representations of the quantified data and representative images are shown (1, 2, 3 refer to three different patients). Data (mean±SEM) were normalized versus the expression of the housekeeping gene/protein GAPDH and expressed as percentage of control (gene expression in the untreated cells were considered 100%). Statistical analysis was performed by repeated measures (RM) one-way ANOVA with Bonferroni's multiple comparison test (*p < 0.05, **p < 0.01, ***p < 0.001, vs Veh). V, vehicle.

Research Grant from the Spanish Ministry of Education, Culture and Sport (FPU16/05896 and FPU18/02435 respectively) and A.M.B holds a Predoctoral Trainee Research Grant from the Spanish Ministry of Science, Innovation and Universities (FPU19/05064).

CRediT authorship contribution statement

Angela B Moragrega: Data curation, Formal analysis; **Aleksandra Gruevska:** Data curation, Formal analysis; **Isabel Fuster-Martínez:** Data curation, Formal analysis; **Ana M. Benedicto:** Data curation, Formal analysis; **Joan Tosca:** Conceptualization, Methodology; **Cristina Montón:** Conceptualization, Methodology; **Victor M. Victor:** Supervision; Validation; **Juan V. Esplugues:** Funding acquisition; **Ana Blas-García:** Funding acquisition, Project administration, Conceptualization. **Nadezda Apostolova:** Funding acquisition, Project administration, Conceptualization, Writing – original draft.

Declaration of Competing Interest

The authors declare that the research was conducted in the absence of any commercial or financial relationships that could be construed as a potential conflict of interest.

Data Availability

Data will be made available on request.

Appendix A. Supporting information

Supplementary data associated with this article can be found in the online version at doi:10.1016/j.biopha.2023.115537.

References

[1] A.M. Moon, A.G. Singal, E.B. Tapper, Contemporary epidemiology of chronic liver disease and cirrhosis, Clin. Gastroenterol. Hepatol. 18 (2020) 2650–2666, https://doi.org/10.1016/j.cgh.2019.07.060.

[2] S.K. Asrani, H. Devarbhavi, J. Eaton, P.S. Kamath, Burden of liver diseases in the world, J. Hepatol. 70 (1) (2019) 151–171, https://doi.org/10.1016/j.jhep.2018.09.014.

[3] T.G. Cotter, M. Rinella, Nonalcoholic fatty liver disease 2020: the state of the disease, Gastroenterology 158 (7) (2020) 1851–1864, https://doi.org/10.1053/j.gastro.2020.01.052.

[4] L. Wiering, F. Tacke, Treating inflammation to combat non-alcoholic fatty liver disease, J. Endocrinol. 256 (1) (2022), e220194, https://doi.org/10.1530/JOE-22-0194.

[5] J.P. Pradere, J. Kluwe, S. De Minicis, J.J. Jiao, G.Y. Gwak, D.H. Dapito, M.K. Jang, N.D. Guenther, I. Mederacke, R. Friedman, A.C. Dragomir, C. Aloman, R. F. Schwabe, Hepatic macrophages but not dendritic cells contribute to liver fibrosis by promoting the survival of activated hepatic stellate cells in mice, Hepatology 58 (4) (2013) 1461–1473, https://doi.org/10.1002/hep.26429.

[6] R.W.M. Min, F.W.M. Aung, B. Liu, A. Arya, S. Win, Mechanism and therapeutic targets of c-Jun-N-terminal kinases activation in nonalcoholic fatty liver disease, Biomedicines 10 (8) (2022) 2035, https://doi.org/10.3390/biomedicines10082035.

[7] C. Baeck, X. Wei, M. Bartneck, V. Fech, F. Heymann, N. Gassler, K. Hittatiya, D. Eulberg, T. Luedde, C. Trautwein, F. Tacke, Pharmacological inhibition of the chemokine C-C motif chemokine ligand 2 (monocyte chemoattractant protein 1) accelerates liver fibrosis regression by suppressing Ly-6C(+) macrophage infiltration in mice, Hepatology 59 (2014) 1060–1072, https://doi.org/10.1002/hep.26783.

[8] J. Ehling, M. Bartneck, X. Wei, F. Gremse, V. Fech, D. Möckel, C. Baeck, K. Hittatiya, D. Eulberg, T. Luedde, F. Kiessling, C. Trautwein, T. Lammers, F. Tacke, CCL2-dependent infiltrating macrophages promote angiogenesis in progressive liver fibrosis, Gut 63 (2014) 1960–1971, https://doi.org/10.1136/gutjnl-2013-306294.

[9] A. Martí-Rodrigo, F. Alegre, A.B. Moragrega, F. García-García, P. Martí-Rodrigo, A. Fernández-Iglesias, J. Gracia-Sancho, N. Apostolova, J.V. Esplugues, A. Blas-García, Rilpivirine attenuates liver fibrosis through selective STAT1-mediated apoptosis in hepatic stellate cells, Gut 69 (5) (2020) 920–932, https://doi.org/10.1136/gutjnl-2019-318372.

[10] F. Lucantoni, A.M. Benedicto, A. Gruevska, A.B. Moragrega, I. Fuster-Martínez, J. V. Esplugues, A. Blas-García, N. Apostolova, Implication of autophagy in the antifibrogenic effect of Rilpivirine: when more is less, Cell Death Dis. 13 (4) (2022), 385, https://doi.org/10.1038/s41419-022-04789-7.

[11] R. Edgar, M. Domrachev, A.E. Lash, Gene expression Omnibus: NCBI gene expression and hybridization array data Repository, Nucleic Acids Res 30 (1) (2002) 207–210, https://doi.org/10.1093/nar/30.1.207.

[12] M. Ashburner, C.A. Ball, J.A. Blake, D. Botstein, H. Butler, J.M. Cherry, A.P. Davis, K. Dolinski, S.S. Dwight, J.T. Eppig, M.A. Harris, D.P. Hill, L. Issel-Tarver, A. Kasarskis, S. Lewis, J.C. Matese, J.E. Richardson, M. Ringwald, G.M. Rubin, G. Sherlock, Gene ontology: tool for the unification of biology, Nat. Genet. 25 (2000) 25–29, https://doi.org/10.1038/75556.

[13] Z.-L. Hu, J. Bao, J.M. Reecy, CateGOrizer: a web-based program to batch analyze gene ontology classification categories, Online J. Bioinforma. 9 (2) (2008) 108–112.

[14] X. Zhang, J. Shen, K. Man, E.S. Chu, T.O. Yau, J.C. Sung, M.Y. Go, J. Deng, L. Lu, V. W. Wong, J.J. Sung, G. Farrell, J. Yu, CXCL10 plays a key role as an inflammatory mediator and a non-invasive biomarker of non-alcoholic steatohepatitis, J. Hepatol. 61 (6) (2014) 1365–1375, https://doi.org/10.1016/j.jhep.2014.07.006.

[15] S. She, L. Ren, P. Chen, M. Wang, D. Chen, Y. Wang, H. Chen, Functional roles of chemokine receptor CCR2 and its ligands in liver disease, Front. Immunol. 13 (2022), 812431, https://doi.org/10.3389/fimmu.2022.812431.

[16] E. Lefebvre, G. Moyle, R. Reshef, L.P. Richman, M. Thompson, F. Hong, H.L. Chou, T. Hashiguchi, C. Plato, D. Poulin, T. Richards, H. Yoneyama, H. Jenkins, G. Wolfgang, S.L. Friedman, Antifibrotic effects of the dual CCR2/CCR5 antagonist cenicriviroc in animal models of liver and kidney fibrosis, PLoS One 11 (6) (2016), e0158156, https://doi.org/10.1371/journal.pone.0158156.

[17] L. Shan, F. Wang, D. Zhai, X. Meng, J. Liu, X. Lv, New drugs for hepatic fibrosis, Front Pharm. 13 (2022), 874408, https://doi.org/10.3389/fphar.2022.874408.

[18] Q.M. Anstee, B.A. Neuschwander-Tetri, W.V. Wai-Sun, M.F. Abdelmalek, G. Rodriguez-Araujo, H. Landgren, G.S. Park, P. Bedossa, N. Alkhouri, F. Tacke, A. J. Sanyal, Cenicriviroc lacked efficacy to treat liver fibrosis in nonalcoholic steatohepatitis: AURORA phase III randomized study, 00273-2, Clin. Gastroenterol. Hepatol. S1542–3565 (23) (2023), https://doi.org/10.1016/j.cgh.2023.04.003.

[19] C.E. Harvey, J.J. Post, P. Palladinetti, A.J. Freeman, R.A. Ffrench, R.K. Kumar, G. Marinos, A.R. Lloyd, Expression of the chemokine IP-10 (CXCL10) by hepatocytes in chronic hepatitis C virus infection correlates with histological severity and lobular inflammation, J. Leukoc. Biol. 74 (3) (2003) 360–369, 10/1189/jlb.0303093.

[20] E. Hintermann, M. Bayer, J.M. Pfeilschifter, A.D. Luster, U. Christen, CXCL10 promotes liver fibrosis by prevention of NK cell mediated hepatic stellate cell inactivation, J. Autoimmun. 35 (4) (2010) 424–435, https://doi.org/10.1016/j.jaut.2010.09.003.

[21] A. Bertola, S. Bonnafous, R. Anty, S. Patouraux, M.C. Saint-Paul, A. Iannelli, J. Gugenheim, J. Barr, J.M. Mato, Y. Le Marchand-Brustel, A. Tran, P. Gual, Hepatic expression patterns of inflammatory and immune response genes associated with obesity and NASH in morbidly obese patients, PLoS One 5 (10) (2010), e13577, https://doi.org/10.1371/journal.pone.0013577.

[22] B. Cicuéndez, I. Ruiz-Garrido, A. Mora, G. Sabio, Stress kinases in the development of liver steatosis and hepatocellular carcinoma, Mol. Metab. 50 (2021), 101190, https://doi.org/10.1016/j.molmet.2021.101190.

[23] Y.-J. Lee, B.-M. Kim, Y.-H. Ahn, J.H. Choi, Y.-H. Choi, J.L. Kang, STAT6 signaling mediates PPARγ activation and resolution of acute sterile inflammation in mice, Cells 10 (3) (2021) 501.

[24] S. Zheng, L. Hoos, J. Cook, G. Tetzloff, H. Davis Jr, M. van Heek, J.J. Hwa, Ezetimibe improves high fat and cholesterol diet-induced non-alcoholic fatty liver disease in mice, Eur. J. Pharmacol. 584 (1) (2008) 118–124, https://doi.org/10.1016/j.ejphar.2008.01.045.

[25] J. Henkel, C.D. Coleman, A. Schraplau, K. Jöhrens, D. Weber, J.P. Castro, M. Hugo, T.J. Schulz, S. Krämer, A. Schürmann, G.P. Püschel, Induction of steatohepatitis (NASH) with insulin resistance in wildtype B6 mice by a western-type diet containing soybean oil and cholesterol, Mol. Med. 23 (2017) 70–82, https://doi.org/10.2119/molmed.2016.00203.

[26] S. Subramanian, L. Goodspeed, S. Wang, J. Kim, L. Zeng, G.N. Ioannou, W. G. Haigh, M.M. Yeh, K.V. Kowdley, K.D. O'Brien, S. Pennathur, A. Chait, Dietary cholesterol exacerbates hepatic steatosis and inflammation in obese LDL receptor-deficient mice, J. Lipid Res. 52 (9) (2011) 1626–1635, https://doi.org/10.1194/jlr.M016246.

[27] Y. Oligschlaeger, R. Shiri-Sverdlov, NAFLD preclinical models: more than a handful, less of a concern? Biomedicines 8 (2) (2020) 28, https://doi.org/10.3390/biomedicines8020028.

[28] A. Spruss, J. Henkel, G. Kanuri, D. Blank, G.P. Püschel, S.C. Bischoff, I. Bergheim, Female mice are more susceptible to nonalcoholic fatty liver disease: sex-specific regulation of the hepatic AMP-activated protein kinase-plasminogen activator inhibitor 1 cascade, but not the hepatic endotoxin response, Mol. Med. 18 (1) (2012) 1346–1355, https://doi.org/10.2119/molmed.2012.00223.

[29] K. Wouters, P.J. van Gorp, V. Bieghs, M.J. Gijbels, H. Duimel, D. Lütjohann, A. Kerksiek, R. van Kruchten, N. Maeda, B. Staels, M. van Bilsen, R. Shiri-Sverdlov, M.H. Hofker MH, Dietary cholesterol, rather than liver steatosis, leads to hepatic inflammation in hyperlipidemic mouse models of nonalcoholic steatohepatitis, Hepatology 48 (2) (2008) 474–486, https://doi.org/10.1002/hep.22363.

[30] L. Recena Aydos, L. Aparecida do Amaral, R. Serafim de Souza, A.C. Jacobowski, E. Freitas Dos Santos, M.L. Rodrigues Macedo, Nonalcoholic fatty liver disease induced by high-fat diet in C57bl/6 models, Nutrients 11 (12) (2019) 3067, https://doi.org/10.3390/nu11123067.

[31] M. Ganz, T. Csak, G. Szabo, High fat diet feeding results in gender specific steatohepatitis and inflammasome activation, World J. Gastroenterol. 20 (26) (2014) 8525–8534, https://doi.org/10.3748/wjg.v20.i26.8525.